

A VoF method for DNS of droplet-laden incompressible turbulence

A. Baraldi* & A. Ferrante**

Corresponding author: ferrante@aa.washington.edu

* Graduate student, Department of Aeronautics & Astronautics, University of Washington, Seattle, USA

** Assistant professor, Department of Aeronautics & Astronautics, University of Washington, Seattle, USA

Abstract: We investigated the continuum surface force (CSF) model to include the surface tension within a projection method combined with a split-advection, mass-conserving, wisps-free volume of fluid (VoF) method that we recently developed to perform DNS of fully-resolved droplet-laden incompressible turbulence. The interface curvature is computed accurately using a variable-stencil height-function technique. We tested different implementations of the surface tension and pressure gradient terms within a projection method, and analyzed their stability and the magnitude of the spurious currents for a static drop in both two and three dimensions. We have modified the sequence of the advection sweeps, and show that, in the case of non-zero Weber number, the algorithm is stable, and the spurious currents maximum magnitude is about 1% of the droplet velocity. Finally, we present DNS results of fully-resolved droplet-laden incompressible isotropic turbulence at $Re_\lambda = 75$ using a computational mesh of 1024^3 grid points and 7000 droplets of Weber number $We = 0.5$, and initial droplet diameter equal to the Taylor length-scale of turbulence.

Keywords: droplet-laden flow, isotropic turbulence, volume of fluid method, continuum surface force.

1 Introduction

In [1], we have recently developed a mass-conserving wisps-free volume of fluid (VoF) method to track volumes in incompressible turbulent flows. The VoF advection is performed through a spatially split approach, the Eulerian implicit - Eulerian algebraic - Lagrangian explicit (EI-EA-LE) algorithm originally proposed by Scardovelli *et al.* [2]. The original EI-EA-LE algorithm is globally mass-conserving but generates wisps and does not conserve the mass of the individual volumes tracked in the flow. Mass conservation properties are guaranteed, and we have improved this method with the addition of a redistribution and a wisps suppression algorithms. Our method is wisps-free and thus conserves mass both globally and locally within each volume tracked.

This paper presents a numerical methodology to perform DNS of uniform-density droplet-laden incompressible turbulent flows. We present and analyze the numerical treatment of the surface tension force within a projection method combined with our VoF method described in [1]. The surface tension effects are treated with the continuum surface force (CSF) approach proposed by Brackbill *et al.* [3] and adapted to the VoF method by Francois *et al.* [4]. We present results for the coupled droplet/fluid flow for a static droplet in 2D and 3D, translating spherical droplet in a uniform flow, 2D droplet in Taylor-Green vortex flow, and droplet-laden isotropic turbulence.

2 Mathematical formulation

2.1 Governing equations

The governing equations for a uniform-density droplet-laden incompressible flow written in non-dimensional form are the continuity,

$$\nabla \cdot \mathbf{u} = 0, \quad (1)$$

and momentum equation,

$$\partial_t \mathbf{u} + \nabla \cdot (\mathbf{u}\mathbf{u}) = -\nabla p + \nu \nabla^2 \mathbf{u} + \mathbf{f}_\sigma, \quad (2)$$

where \mathbf{f}_σ is the force per unit mass due to the droplet surface tension, σ , and the non-dimensional density is omitted because equal to one ($\rho_d = \rho = 1$).

2.2 Numerical method

2.2.1 Projection method

We now present the projection method to solve the governing equations (1) and (2). Time integration of (2) is performed using the second-order Adams-Bashforth scheme,

$$\frac{\mathbf{u}^* - \mathbf{u}^n}{\Delta t} = \frac{3}{2} \mathbf{R}\mathbf{U}^n - \frac{1}{2} \mathbf{R}\mathbf{U}^{n-1}, \quad (3)$$

to compute \mathbf{u}^* that is a non-divergence free approximate fluid velocity, and where

$$\mathbf{R}\mathbf{U}^n = -\nabla \cdot (\mathbf{u}^n \mathbf{u}^n) + \nu \nabla^2 \mathbf{u}^n + \mathbf{f}_\sigma^{n+1}. \quad (4)$$

The divergence-free condition on the updated fluid velocity is imposed by solving the Poisson equation for pressure,

$$\nabla^2 p^{n+1} = \frac{1}{\Delta t} \nabla \cdot \mathbf{u}^*, \quad (5)$$

and by updating the fluid velocity as

$$\mathbf{u}^{n+1} = \mathbf{u}^* - \Delta t \nabla p^{n+1}. \quad (6)$$

Equations (4), (5) and (6) are discretized in space on a uniform staggered mesh using second-order central difference schemes. The Poisson equation (5) in finite-difference form is solved using a combination of a two-dimensional fast Fourier transform (FFT) in the $x - y$ plane, and Gauss elimination in the z direction. Periodic boundary conditions are imposed in the three directions. In Eq. (3), the surface tension term, \mathbf{f}_σ , is computed using the continuous surface force (CSF) approach by Brackbill *et al.* [3] as

$$\mathbf{f}_\sigma = \sigma \kappa \mathbf{n}, \quad (7)$$

where σ is the droplet surface tension, κ is the local curvature of the interface between droplet and surrounding fluid, and \mathbf{n} is the local unit normal to the droplet/fluid interface. Francois *et al.* [4] reformulated the CSF by replacing \mathbf{n} with the gradient of the volume fraction or VoF function, C . Such to satisfy a consistent coupling of the surface tension force with pressure gradient force within the flow solver, \mathbf{f}_σ is computed at the cell faces as [4]

$$\mathbf{f}_\sigma = \sigma \kappa \nabla C. \quad (8)$$

Thus, the computation of \mathbf{f}_σ requires the computation of κ and C . The next two sections are dedicated to the descriptions for computing C , using the volume of fluid method by [1], and κ , using the height-function technique by [5].

2.2.2 Volume of fluid method

We developed a novel volume of fluid (VoF) method [1] that is mass-conserving and wisps-free. The complete details of the VoF method are given by Ferrante & Baraldi [1]. A brief description is here reported.

In the volume of fluid (VoF) method, the sharp interface between the two phases (e.g. liquid and gas) is determined using the VoF function, C , that represents the volume fraction of the reference phase in each computational cell, e.g. $C = 0$ in the surrounding fluid, and $C = 1$ inside the droplet ($0 \leq C \leq 1$).

The VoF method is characterized by a sharp representation of the interface. In the present VoF method, the interface between the two phases is reconstructed using a piecewise linear interface calculation (PLIC) [6]. The reconstruction of the interface in each computational cell consists of two steps: the computation of the interface normal, $\mathbf{n} = (n_x, n_y, n_z)$, and the computation of the interface location. The algorithm that we use to evaluate the interface normal is a combination of the centered-columns method [7] and Youngs' method known as the mixed-Youngs-centered (MYC) method [8].

Considering a characteristic function χ that has value 1 inside the droplet and 0 in the surrounding fluid, the phase of interest moves obeying the following advection equation:

$$\frac{\partial \chi}{\partial t} + \mathbf{u} \cdot \nabla \chi = 0. \quad (9)$$

The volume fraction $C_{i,j,k}$ of grid cell i, j, k is related to the characteristic function χ by the integral relation

$$C_{i,j,k}(t) = \frac{1}{V_0} \int_{V_0} \chi(\mathbf{x}, t) d\mathbf{x}, \quad (10)$$

where V_0 is the volume of the i, j, k cell.

The VoF advection step to advance C in time is performed with the Eulerian implicit - Eulerian algebraic - Lagrangian explicit (EI-EA-LE) algorithm originally proposed by Scardovelli *et al.* [2]. The original EI-EA-LE algorithm is globally mass-conserving but generates wisps and does not conserve the mass of the individual volumes tracked in the flow. We have improved this method with the addition of a redistribution and a wisp suppression algorithms. The redistribution algorithm is needed since small inconsistencies in the VoF values (i.e. $C < 0$ and $C > 1$) can arise in the Eulerian algebraic (EA) step of the advection. A wisp suppression algorithm has also been developed in order to correct the solution from small errors arising from the finite machine precision (Fig. 1). Our method is wisps-free and thus conserves mass both globally and locally within each droplet. The advection of C is performed using a staggered mesh discretization of the velocity field with respect to C . The method displays second-order spatial accuracy and almost second-order overall accuracy for typical values of the CFL number used in the test-case simulations as shown in Fig. 2. A geometrical error smaller than 1% is obtained with a droplet resolution of 30 grid cells or more across the diameter.

2.2.3 Curvature computation

In order to compute the interface curvature from the VoF function, C , the height function technique by Cummins *et al.* [5] has been adopted and investigated. A correction based on the local orientation of the interface normal is performed to minimize the error on a spherical interface. The technique is second-order accurate with respect to the mesh size and is computationally efficient. The height function is constructed by integrating the C along the axis direction for which the normal to the interface has the largest component. The method relies solely on the discrete values of C , and is mostly independent from the interface normal computation, which only influences the orientation of the curvature computational stencil, thus, making the method robust. The interface normal is computed using the mixed-Youngs-Centered (MYC) method on a uniform Cartesian mesh. For example, consider the case with the interface normal with the largest component in the z -direction. Then, the local height function H in the (i, j, k) cell containing the interface (because $0 < C_{i,j,k} < 1$) is computed along z on a 3×3 computational stencil in the $x - y$ plane for a fixed κ value as

$$H_{r,s} = \sum_{t=t_{down}}^{t_{up}} C_{i+r,j+s,k+t}^* \Delta x \quad \text{with} \quad r = [-1, 0, 1] \quad \text{and} \quad s = [-1, 0, 1] \quad (11)$$

where t_{up} and t_{down} are adjusted adaptively based on the local C distribution (t_{up} can vary from 0 to 3, and t_{down} can vary from -3 to 0), and C^* is a modified distribution of the volume fraction C , which is rendered

monotonic along the z -direction [9]. The stencil for computing H in the i, j, k cell is therefore of variable size and ranges from $3 \times 3 \times 1$ to $3 \times 3 \times 7$. The interface curvature is then computed using the height function H as

$$\kappa = \frac{n_z}{|n_z|} \frac{H_{xx} + H_{yy} + H_{xx}H_y^2 + H_{yy}H_x^2 - 2H_{xy}H_xH_y}{(1 + H_x^2 + H_y^2)^{3/2}}, \quad (12)$$

where the partial derivatives of H are computed using the finite difference formula of [9]. These formulas introduce extra staggered terms weighed by a parameter γ which improves the accuracy in three dimensions. The discretized first derivative of H is written as

$$H_x = \frac{[\gamma(H_{1,1} - H_{-1,1}) + H_{1,0} - H_{-1,0} + \gamma(H_{1,-1} - H_{-1,-1})]}{2\Delta x(1 + 2\gamma)}, \quad (13)$$

and the discretized second derivative of H as

$$H_{xx} = \frac{[\gamma(H_{1,1} - 2H_{0,1} + H_{-1,1}) + H_{1,0} - 2H_{0,0} + H_{-1,0} + \gamma(H_{1,-1} - 2H_{0,-1} + H_{-1,-1})]}{\Delta x^2(1 + 2\gamma)}. \quad (14)$$

Lopez and Hernandez [9] define the parameter γ as

$$\gamma = 0.2 \quad \text{if} \quad \arccos(\max(|n_x|), \max(|n_y|), \max(|n_z|)) > 0.8 \quad (15)$$

$$\gamma = 0 \quad \text{if} \quad \arccos(\max(|n_x|), \max(|n_y|), \max(|n_z|)) \leq 0.8. \quad (16)$$

The cross derivative H_{xy} is calculated as

$$H_{xy} = \frac{H_{1,1} - H_{1,-1} - H_{-1,1} + H_{-1,-1}}{4\Delta x^2}. \quad (17)$$

Note that the condition $\arccos(\max(|n_x|), \max(|n_y|), \max(|n_z|)) > 0.8$ occurs when the interface normal is not aligned predominantly to any of the three directions, causing a loss of accuracy in the height function method. We found that the accuracy of the computed κ can be further improved where $\arccos(\max(|n_x|), \max(|n_y|), \max(|n_z|)) > 0.95$ by computing three height functions, one for each direction, by computing three curvatures associated with each height function (12), and by taking the mean value of the three computed curvatures.

3 Results

In this section, we report the results of the performed simulations for the following uniform-density coupled droplet/fluid flows: static droplet (2D and 3D), spherical droplet translating in a uniform flow, droplet in a Taylor-Green vortex flow, and droplet-laden isotropic turbulence.

3.1 Static droplet

3.1.1 2D static droplet

We tested the numerical method described in Sec. 2.2 to compute the coupled fluid/droplet flow for the case of a viscous droplet at rest in a quiescent fluid, i.e. static droplet. The droplet-at-rest case proves to be a very good test in order to assess the characteristics of the two-phase flow solver, in particular its ability to obtain a balance between pressure gradient and surface tension across the interface. This test-case is relevant because the numerical solution should stay constant in time, however the so-called spurious currents are generated in the flow field as shown in Fig. 4. For that case with a droplet resolution of 32 cells across the diameter and $\Delta t/\Delta x = 0.01$, Table 1 reports the values of the maximum spurious currents averaged over 1000 time steps as a function of the non-dimensional surface tension coefficient σ .

σ	cylinder $ u _{max}$	sphere $ u _{max}$
5	7.15e-4	2.46e-3
0.5	2.46e-4	1.02e-3
0.05	7.59e-5	3.30e-4

Table 1: Time-averaged maximum spurious currents for a viscous droplet at rest for different values of the non-dimensional surface tension coefficient, σ .

These results are consistent with those reported in the literature by [4] and [9]. Also, the magnitude of these currents is negligible if the analytical curvature was imposed at the interface cells for computing \mathbf{f}_σ in (8) as shown in Fig. 5. This proves that the method is consistent and a balance between pressure gradient and surface tension holds if the curvature is exact. However, in addition to the findings of [4] and [9], we have noted that by running the simulation for several thousands of time steps, the flow field velocities can suddenly grow to higher values and then keep oscillating around a higher mean value. Figure 6 shows the time history of spurious currents and pressure for the case of a 2D viscous static droplet of diameter $D = 0.5$ and $\sigma = 5$ at rest in a 1×1 square domain with a 64×64 mesh resolution (circular droplet). Figure 6 shows also the time history of the sum of the 2D velocity components U and W in the field, which is expected to be zero if the resulting flow field was 4-fold symmetric. Since these sums are non-zero and grow in time, the flow field is not 4-fold symmetric. In order to investigate the source of these asymmetries in the flow field and if they were caused by the split VoF advection algorithm, we repeated the test case, this time enforcing a 4-fold symmetry only to the VoF function, C . The results show that no asymmetries develop in the flow field, and the spurious currents magnitude decreases in time, see Fig. 7. This proves that the magnitude of the spurious currents grows in time in Fig. 6 because of the asymmetry in the flow that develops within the split VoF method in the C field.

3.1.2 3D static droplet

Similar results to those described for the 2D static droplet were obtained for the 3D static (spherical) droplet. Figures 8 and 9 show, respectively, the magnitude of the spurious currents of the solver without and with imposed symmetry of the VoF function. In the 3D case, the symmetry was enforced by mirroring C onto the 8 different quadrants of the mesh centered at the spherical drop center (8-fold symmetry). When symmetry is enforced on the VoF function, the spurious currents magnitude decreases in time.

Based on what we learned from the static droplet numerical tests, we modified the VoF advection algorithm, trying to reduce the directionality of the 1D advection steps. Initially, the EI-EA-LE advection steps were cycled amongst the three spatial directions in a simple way, by assigning the first EI sweep to a different direction at each time step. We tried more complex combinations for this assignment, and this resulted to be beneficial in delaying the growth of the spurious currents in the static drop case. This is because the advection algorithm becomes more and more ‘isotropic’.

3.2 Spherical droplet translating in a uniform flow

In this test case, we prescribed a uniform velocity throughout the computational domain including the interior of the droplet initially placed at the center of the computational domain. No symmetry in the VoF distribution was enforced for this case. The results show that there are no instabilities in the case of non-zero Weber number, e.g. when a mean droplet velocity is present. The algorithm proves to be stable, and the spurious currents are of the order of 1% of the translating velocity, as shown in Fig. 10.

3.3 2D circular droplet in Taylor-Green vortex flow

We have then tested the numerical method with a 2D droplet in a Taylor-Green vortex flow. Figure 11 shows the instantaneous pressure contours, streamlines and droplet/fluid interface ($C = 0.5$ isoline) in the coupled droplet/Taylor-Green vortex flow at four different times. The solution is stable after several thousands of time steps, the droplet interface remains smooth in time, and spurious velocities are undetectable in the flow field.

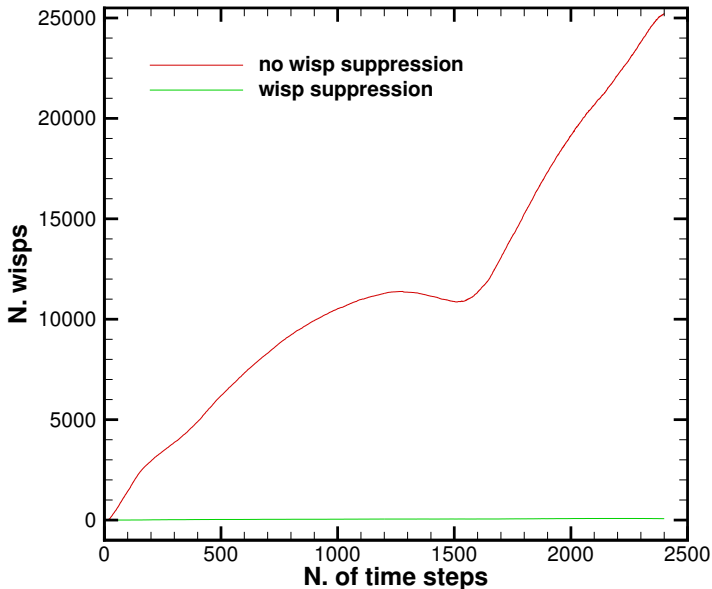


Figure 1: Total number of wisps vs number of time steps for a sphere of radius 0.15 advected in a time reversed single-vortex field [10] with period $T=2$ using a mesh of 128^3 grid points.

3.4 Droplet-laden isotropic turbulence

In Fig. 12, we present DNS results of fully-resolved droplet-laden incompressible decaying isotropic turbulence at an initial Reynolds number based on Taylor length-scale of turbulence $Re_\lambda = 75$ using a computational mesh of 1024^3 grid points and 7000 droplets. The droplet Weber number based on the r.m.s. velocity fluctuation of turbulence is $We = 0.5$, the initial droplet diameter is equal to the Taylor length-scale of turbulence, and the droplet volume fraction is $\phi = 0.1$. The curvature contours in Fig. 12 show that the droplets curvature variations can reach and exceed 10% of the initial curvature (red and blue regions).

4 Conclusions

We have developed a projection method including a mass-conserving, wisps-free VoF method that we recently developed [1] and the continuous surface force (CSF) model [3] according to [4] to simulate uniform-density droplet-laden incompressible flows. We have tested the numerical method in several test cases such as the static droplet. Such tests have helped us to improve the accuracy of the methodology by performing the EI step of the split advection algorithm not in a standard fashion, and to evaluate the average curvature of three computed when the $\arccos(\max(|n_x|), \max(|n_y|), \max(|n_z|)) > 0.95$. Finally, we have applied the method to a complex flow such as droplet-laden isotropic turbulence. Next, we will extend this method to variable-density droplet-laden flows within our parallel DNS computational framework for simulating droplet-laden isotropic turbulence.

This work was supported by the National Science Foundation CAREER Award (OCI-1054591). The simulations were performed in part on a high-performance computer cluster called Hyak at the University of Washington, Seattle. This research was supported in part by the National Science Foundation through the XSEDE computational resources provided by the National Institute for Computational Sciences (NICS) at the Oak Ridge National Laboratory, under XSEDE grant number TG-CTS100024. We specifically acknowledge the assistance of the XSEDE ECSS team members, Jay Alameda and Darren Adams, of the National Center for Supercomputing Applications (NCSA) at the University of Illinois at Urbana-Champaign.

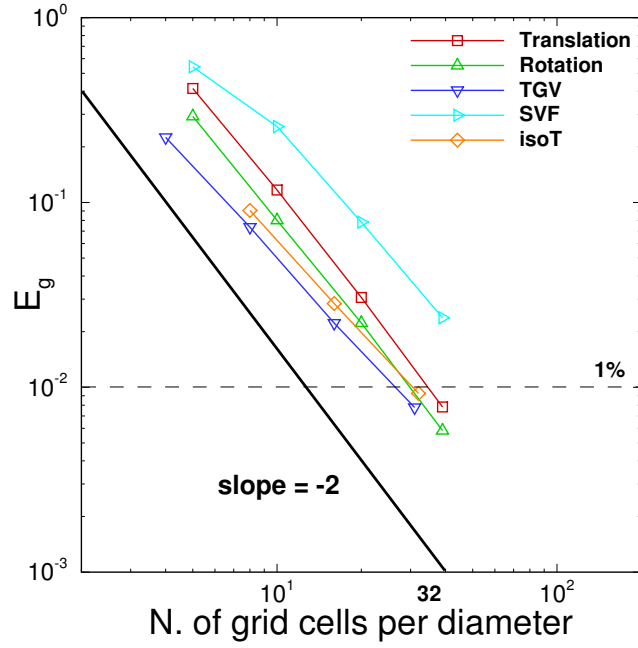


Figure 2: Geometrical error, E_g , of the advection and reconstruction algorithm for a sphere as a function of mesh resolution at CFL=0.1. Translation along the box diagonal, rotation and time-reversed single-vortex flow (SVF) with period $T=2$ for a sphere of radius 0.15. Time-reversed Taylor-Green vortex flow (TGV) with period $T=2$ for a sphere of radius 0.12. Time-reversed isotropic turbulence flow at $Re_{\lambda_0} = 75$ (isoT) with period $T=1$.

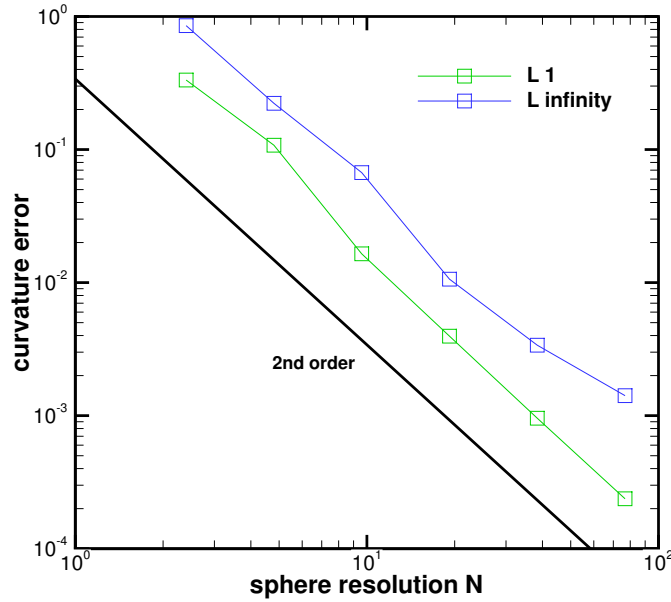


Figure 3: L_1 and L_∞ curvature error norms averaged over 100 randomly placed spheres as a function of the number of grid points per sphere diameter.

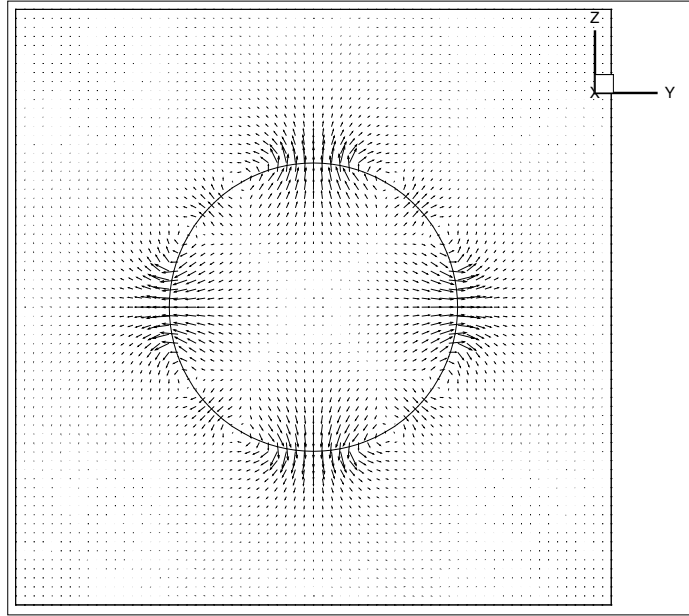


Figure 4: Spurious currents for the viscous 2D static droplet test with $We_D = 1$, $N = 64$, $D = 0.5$: $C = 0.5$ isoline and fluid velocity vectors after 640 time steps.

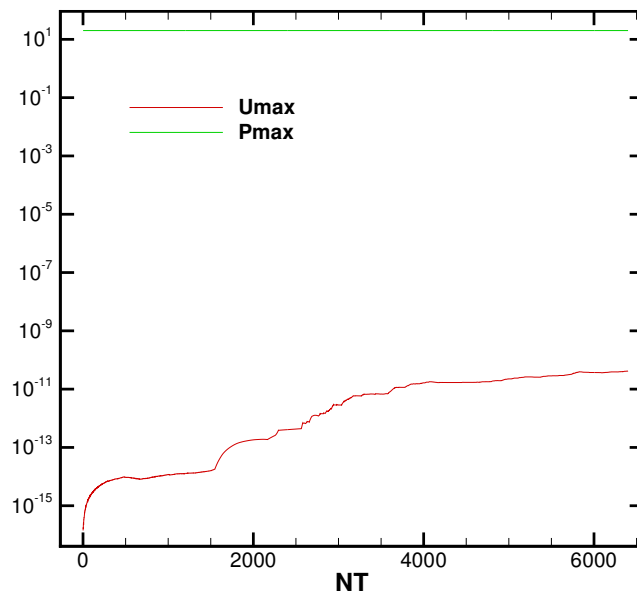


Figure 5: 2D viscous static droplet test at $\sigma = 5$, $N = 64$, $D = 0.5$ using the analytical curvature for computing \mathbf{f}_σ in (8).

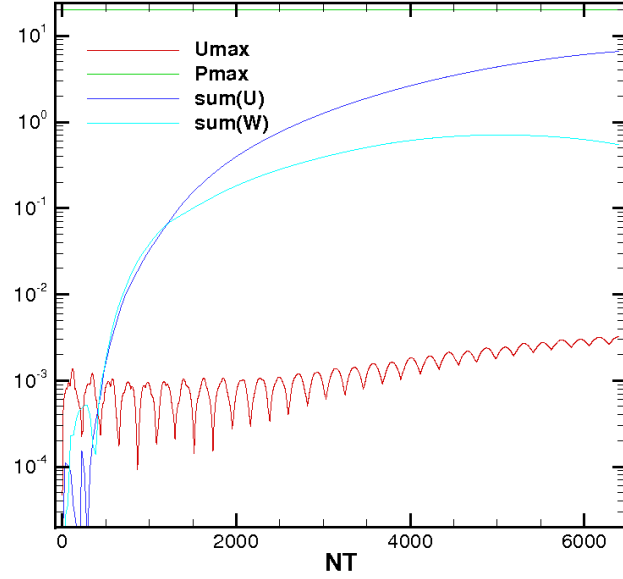


Figure 6: 2D viscous static droplet test at $\sigma = 5$, $N = 64$, $D = 0.5$.

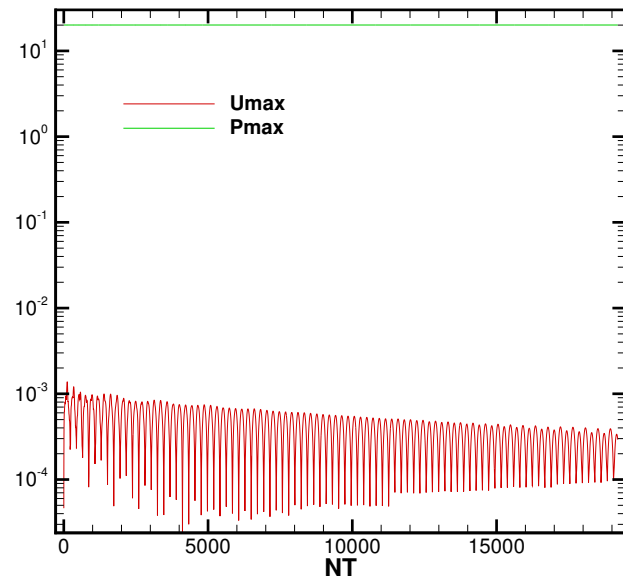


Figure 7: 2D viscous static droplet test at $\sigma = 5$, $N = 64$, $D = 0.5$. 4-fold symmetry is enforced at each time step to the VoF function, C .

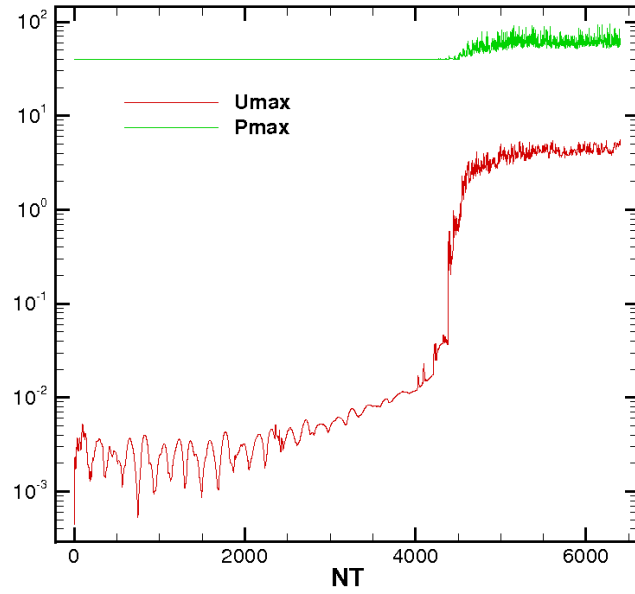


Figure 8: 3D viscous static droplet test at $\sigma = 5$, $N = 64$, $D = 0.5$.

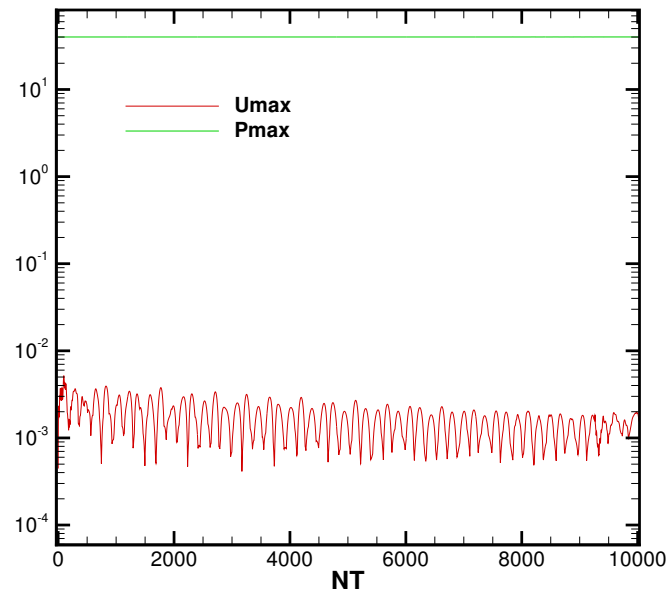


Figure 9: 3D viscous static droplet test at $\sigma = 5$, $N = 64$, $D = 0.5$. 8-fold symmetry enforced to the VoF function, C .

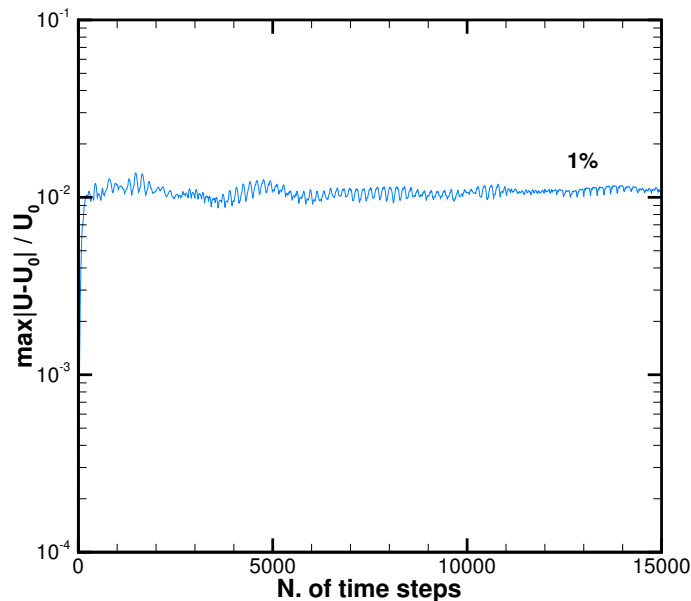


Figure 10: Velocity oscillations (spurious currents) for a translating sphere along the box diagonal, as a function of time.

References

- [1] A. Ferrante and A. Baraldi. A mass-conserving volume of fluid method for DNS of two-phase incompressible isotropic turbulence. *20th AIAA Computational Fluid Dynamics Conference, Honolulu (HI), June 27-30*, 3829:1–16, 2011.
- [2] R. Scardovelli, E. Aulisa, S. Manservigi, and V. Marra. A marker-VOF algorithm for incompressible flows with interfaces. In *Advances in Free Surface and Interface Fluid Dynamics*, volume 1, pages 905–910. ASME Conf. Proc., Joint U.S.-European Fluids Engineering Division Conference, 2002.
- [3] J.U. Brackbill, D.B. Kothe, and C. Zemach. A continuum method for modeling surface tension. *J. Comput. Physics*, 100(2):335–354, 1992.
- [4] M.M. Francois, S.J. Cummins, E.D. Dendy, D.B. Kothe, J.M. Sicilian, and M.W. Williams. A balanced-force algorithm for continuous and sharp interfacial surface tension models within a volume tracking framework. *J. Comput. Physics*, 213(1):141–173, 2006.
- [5] S.J. Cummins, M.M. Francois, and D.B. Kothe. Estimating curvature from volume fractions. *Computers & structures*, 83(6-7):425–434, 2005.
- [6] DL Youngs. Time-dependent multi-material flow with large fluid distortion. *Numer. Methods for Fluid Dynamics*, 1(1):41–51, 1982.
- [7] G.H. Miller and P. Colella. A Conservative Three-Dimensional Eulerian Method for Coupled Solid-Fluid Shock Capturing* 1. *J. Comput. Physics*, 183(1):26–82, 2002.
- [8] E. Aulisa, S. Manservigi, R. Scardovelli, and S. Zaleski. Interface reconstruction with least-squares fit and split advection in three-dimensional Cartesian geometry. *J. Comput. Physics*, 225(2):2301–2319, 2007.
- [9] J. López and J. Hernández. On reducing interface curvature computation errors in the height function technique. *J. Comput. Physics*, 229:4855–4868, 2010.
- [10] W.J. Rider and D.B. Kothe. Reconstructing volume tracking. *J. Comput. Physics*, 141(2):112–152, 1998.

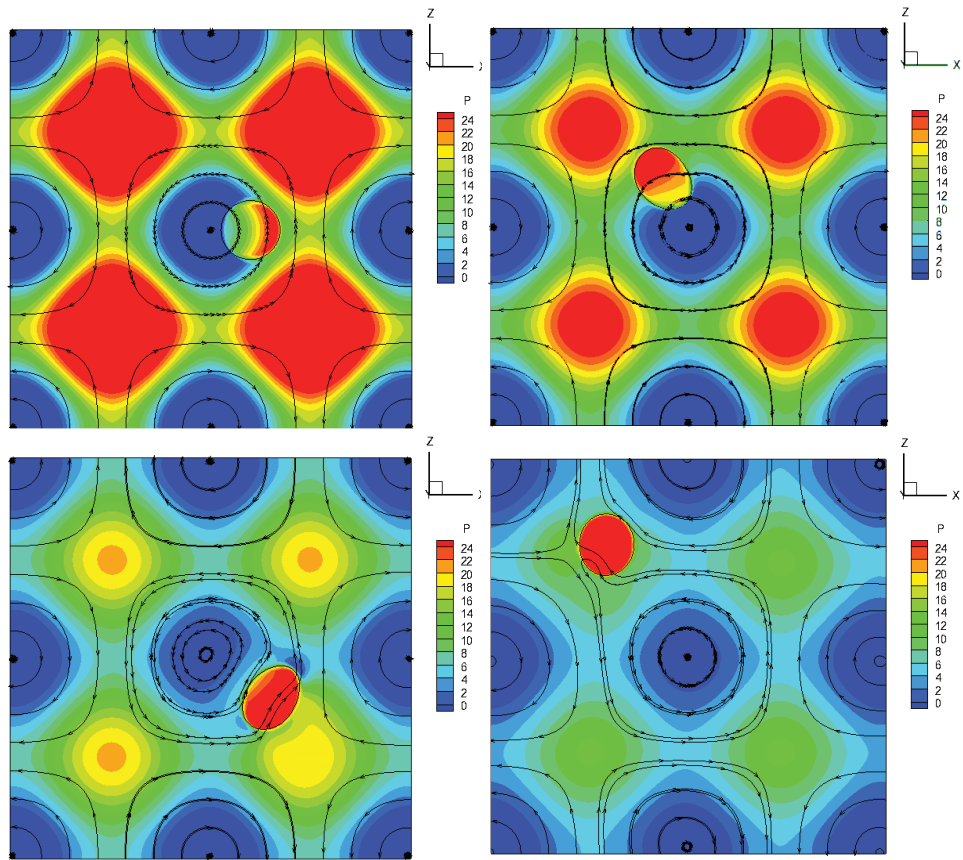


Figure 11: Instantaneous pressure contours, streamlines and droplet/fluid interface ($C = 0.5$ isoline) for a droplet in the Taylor-Green vortex flow ($We_D = 0.1$, $N = 128$, $D = 0.15$) at four different times.

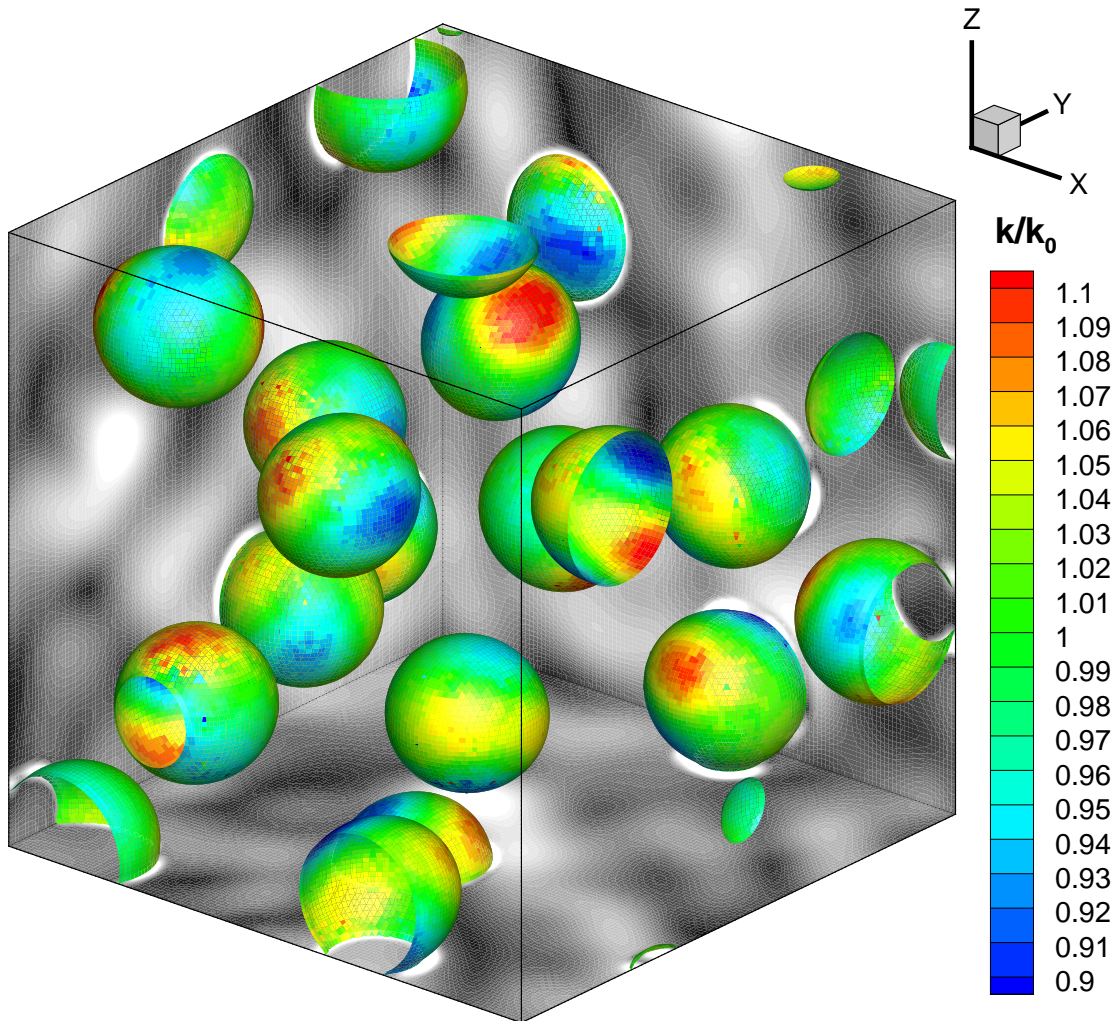


Figure 12: Fully coupled droplet-laden decaying isotropic turbulence ($Re_\lambda = 75$) laden with 7000 droplets. $C = 0.5$ iso-surface with normalized curvature color contours (k/k_0 where k_0 is the initial curvature of the spherical droplets) and vorticity magnitude contours (gray scale). The Weber number based on *r.m.s* velocity and droplet diameter is 0.5, the volume fraction is $\phi = 0.1$, and the droplet resolution is 32 cells across the initial diameter. The plotted region is a 512^{th} of the entire cubic box simulated using a mesh of 1024^3 grid points.